

1 **Interaction between East Asian summer monsoon and westlies as**
2 **shown by tree-ring records**

3

4 Xiao Shengchun^{1*}, Peng Xiaomei¹, Tian Quanyan¹, Ding Aijun², Xie Jiali¹, Su
5 Jingrong^{1,3}

6

7 ¹ Key Laboratory of Ecological Safety and Sustainable Development in Arid Lands,
8 Northwest Institute of Eco-Environment and Resources, Chinese Academy of
9 Sciences, Lanzhou, Gansu, China 730000.

10 ² College of Resources and Environment, Gansu Agricultural University, Lanzhou,
11 Gansu, China 730070.

12 ³ University of Chinese Academy of Sciences, Beijing, China 100049.

13 * Corresponding author (xiaosc@lzb.ac.cn).

14 Address: 320 West Donggang Road, Lanzhou City, Gansu Province, China.

15 Zip Code: 730000.

16

17 **Abstract:**

18 Atmospheric circulation changes, their driving mechanisms and interactions are
19 important topics in global change research. Local changes in the East Asian summer
20 monsoon (EASM) and the mid-latitude westerlies will inevitably affect the climate and
21 ecology of the arid zone of Northwest China. Hence, it is important to study these
22 regional changes. While previous studies in this area are all single-point climate
23 reconstruction studies, there is a lack of research on the interaction areas and driving
24 mechanisms of the two major circulations. Dendroclimatology can provide high-
25 resolution, long-term, and reliable multi-point proxies for the study of inter-annual and
26 inter-decadal climate change. We chose to observe these changes in the Alxa Plateau
27 using dendrochronological methods. We assembled ring-width records of Qinghai
28 spruce (*Picea crassifolia*) in the mountain regions surrounding the Alxa Plateau: the
29 Helan Mountains, Changling Mountain, and Dongdashan Mountain. The results show
30 that radial growth was indeed affected by changes in the monsoon and westerlies. The
31 heterogeneity of precipitation and climatic wet-dry changes in different regions is
32 primarily influenced by the interactions between atmospheric circulation systems, each
33 with its own dominant controlling factors. In the case of the Helan Mountains, both of
34 these major atmospheric circulation systems play a significant role in shaping climate
35 changes. Changling Mountain in the southern part of the Alxa Plateau is mainly
36 influenced by the EASM. Dongdashan Mountain is mainly influenced by the westerlies.
37 Understanding these local conditions will help us predict climate changes in Northwest
38 China.

39

40 **Key words:** Alxa Plateau, dendroclimatology, westerlies, EASM, interaction between
41 winds and monsoon.

42

43 **1. Introduction**

44 The alpine zone of Qinghai-Tibet, the arid zone of the northwestern interior, and
45 the humid zone of the east constitute the three main areas of China's natural
46 geomorphology (Chen et al., 2019a). The Northwest China inland dry zone is located
47 in the hinterland of the Eurasian continent and is among the driest regions in the world.
48 It displays typical climatic characteristics of a continental climate. This region is mainly
49 influenced by the westlies and the East Asian summer monsoon (EASM). The
50 interaction of these two factors results in high precipitation variability and hence
51 frequent droughts. This was true even before the onset of global climate change in the
52 area, and it is even more pronounced in recent years. This inland arid zone is
53 ecologically fragile (Chen et al., 2019a; Chen et al., 2019b; Zhang et al., 2023).

54 The semi-arid and arid regions of northern China are characterized by large areas
55 of sand and desert. They are the second largest source of dust in the world after the
56 Sahara. Their contribution to global climate change is large. So far inland, the influence
57 of the EASM is often weak (Zhang et al., 2021; Liu et al., 2022). It is opposed by the
58 westerlies that flow from the North Atlantic climate zone toward the East Asian
59 monsoon climate zone (Qu et al., 2004). The interaction between the westerlies and the
60 EASM governs precipitation, water vapor transport, and thus the climate of
61 northwestern China (Feng et al., 2004; Wang et al., 2005; Li et al., 2008; Ma et al.,
62 2011).

63 To estimate the impact of global change on this interaction, it is crucial to
64 comprehend its historical context. Global atmospheric circulation is likely to change,
65 as is the EASM. Climate change will not only affect the regional climate and regional
66 water resources (Ding et al., 2023); it will affect East Asia (dust storms) and even the
67 rest of the globe. Hence, the study of climate in this region is of great practical and
68 theoretical significance (Chen et al., 2019a; Chen et al., 2019b).

69 The westerlies and the EASM meet at the northern boundary of the Asian summer
70 monsoon (Huang et al., 2023). In northern China, this boundary runs from west to east,
71 along the eastern section of the Qilian Mountains, the southern foothills of the Helan
72 Mountains, the Daqing Mountains, and the western section of the Daxinganling

73 Mountains. This is not a static boundary. It fluctuates within a range of 200–700 km
74 (Chen et al., 2018). It is important to understand the history of these fluctuations (Huang
75 et al., 2023).

76 This can be done using climate records such as lacustrine, eolian, and
77 dendrochronological (Sun et al., 2003; Liu et al., 2005; Li, 2009; Chen et al., 2010; Li
78 et al., 2016; Chen et al., 2019b; Qin et al., 2023). Dendrochronology is one of the best
79 tools for studying paleoclimatic changes, due to its precise dating, high resolution, good
80 continuity and high replication (Zhang et al., 2003; Shao et al., 2010; Yang et al., 2014;
81 Liu et al., 2016).

82 The climate history of the Baotou area, at the northern edge of the EASM, has been
83 studied at interannual and interdecadal scales for the past 260 years, based on June–
84 August precipitation reconstruction from tree-ring samples from the western Yinshan
85 Mountains (Liu et al., 2001; Liu et al., 2003). Using tree-rings and historical records,
86 Kang and Yang (2015) reconstructed the annual precipitation history of the East Asian
87 monsoon northern fringe zone for the last 530 years. They analyzed spatial variability
88 and possible driving mechanisms using the 400-mm isohyet.

89 Several May–July precipitation sequences have been reconstructed using ring-
90 width and latewood-width data from Chinese pine (*Pinus tabulaeformis*) growing in
91 the Helan Mountains (Ma et al., 2003; Liu et al., 2004; Chen et al., 2016). Studies of
92 tree-ring carbon and oxygen isotopes from Chinese pine samples have shown that $\delta^{18}\text{O}$
93 values increase with summer precipitation, while $\delta^{13}\text{C}$ values decrease (Zhang et al.,
94 2005a; Liu et al., 2008). westerlies have also been shown to affect precipitation in the
95 Helan Mountains (Chen et al., 2010).

96 Principal component analysis of tree-ring chronologies constructed from data
97 collected at several sites in Gansu suggests that trees at these sites were more influenced
98 by EASM than by westerlies (Chen et al., 2013). These researchers also found that the
99 EASM weakened in 1970s, but recovered in the early 1990s. Tree-ring data allowed the
100 reconstruction of 330 years of PDSI (Palmer Drought Severity Index) values for the
101 Mount Hasi region (at the northern boundary of the summer monsoon zone) (Kang et
102 al., 2012). This study confirmed that radial growth of Chinese pine has declined over

103 the past three decades, due to the weakening of the EASM. Dendrochronological
104 reconstruction of precipitation in the Mount Changling region (again using Chinese
105 pine) suggested that precipitation in that region mainly depends on the EASM (Chen et
106 al. 2012). Other researchers have assembled tree-ring chronologies from pines growing
107 in the Mount Qilian region and the northern mountains of the Hexi Corridor. Here again
108 precipitation is associated with the EASM. These chronologies have allowed scholars
109 to compile precipitation, temperature, and drought records for the last thousand years
110 (Gou et al., 2015a; Gou et al., 2015b; Zhang et al., 2017).

111 Most modern researchers studying climate change in the region are mostly carried
112 out on single sample sites (Wang et al., 2004; Liu et al., 2005; Chen et al., 2010; Chen
113 et al., 2016; Li et al., 2016; Liu et al., 2016; Chen et al., 2018). While, there is a dearth
114 of multi-site, regional and long time scale studies on the interaction of the westerlies
115 and the EASM. The research focuses on the interplay area, and investigates the
116 spatiotemporal heterogeneity in climate change and its dominant driving factors,
117 specifically related to the westerlies and East Asia monsoon circulation in Alxa Plateau.

118 Qinghai spruce (*Picea crassifolia*) is a common tree species in the Helan, Changling
119 and Dongdashan mountain areas around the Alxa Plateau. Using dendrochronological
120 methods, we analyzed the climate response characteristics of spruce radial growth on
121 the above three mountains. Combining the relevant Westerly and East Asia monsoon
122 circulation indices, the driving mechanism of the regional climate change by with the
123 interaction and synergistic roles of two atmospheric circulation systems in the Alxa
124 Plateau was explored. The results will lay a theoretical foundation for the climatic
125 evolution of the region and the desertification control.

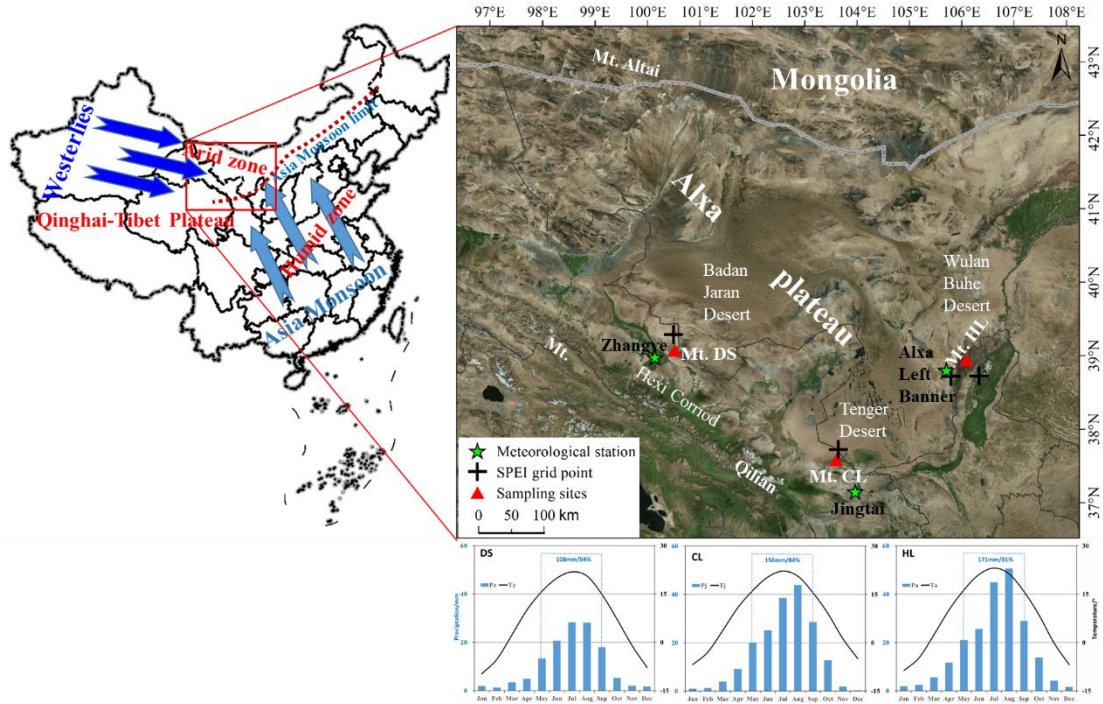
126

127 **2. Material and methods**

128 **2.1 Study area**

129 The Alxa Plateau is located in the western part of the Inner Mongolia Autonomous
130 Region and is surrounded by mountains (Fig.1). It consists primarily of three deserts:
131 Tengger, Ulan Buh, and Badan Jaran. It lies south of the Gobi desert. It is the main
132 source of the fierce sandstorms and dust storms that blow toward eastern China and the

133 Pacific. It has been much affected by climate change; sand- and dust storms have
 134 increased, much to the detriment of lands to the east. The Chinese government is doing
 135 what it can to establish an environmental defense line there. It is currently the Northern
 136 Sand Prevention Belt of the National Two Ecological Barrier and Three Belts
 137 Ecological Security Strategy Pattern (Xiao et al., 2017; Xiao et al., 2019).



138
 139 Figure 1. Location of tree-ring sampling sites and climatic diagram of study area (the upper right
 140 panel is from Mapworld). Pa/Ta are the monthly total precipitation and monthly mean temperature
 141 at the Alxa Left Banner meteorological station (1953–2016); Pj/Tj are the precipitation and
 142 temperature figures for the Jingtai meteorological station (1957–2017); Pz/Tz are the precipitation
 143 and temperature figures for the Zhangye meteorological station (1957–2017). The dashed box and
 144 appended data indicate the total growing season precipitation in the study area and the proportion
 145 of total annual precipitation.

146
 147 There are several mountain ranges surrounding the Alxa Desert, such as the Helan
 148 Mountains in the east, the northern mountains of the Hexi Corridor, and the outliers of
 149 the Altai Mountains in the north. These mountains not only block the eastward and
 150 southward expansion of the desert (driven by high pressure regions from Mongolia);

151 they are also the source of mountain rivers and streams that water the oases on the
152 plateau.

153 The Alxa Plateau is located in the eastern margin of the inland arid region of Central
154 Asia. It is affected not only by the mid-latitude westerly circulation, but also by the
155 Asian monsoon and the Tibet plateau monsoon. It is in the zone where the mid-latitude
156 westerly circulation and the Asian monsoon interact (Xiao et al., 2017; Chen et al.,
157 2019b). As a result, vegetation cover in this region there is characterized by
158 pronounced interannual variability (Ou and Qian, 2006; Tang et al., 2006; Li et al.,
159 2013).

160 The Helan Mountains ($38^{\circ}27' \sim 39^{\circ}30'N$, $105^{\circ}20' \sim 106^{\circ}41'E$) (sampling site
161 henceforth abbreviated as HL), are located at the eastern edge of the Tengger Desert.
162 They stretch more than 200 kilometers from north to south; the main peak is $\sim 3,556$ m.
163 The mountain forests are dominated by Qinghai spruce and Chinese pine, juniper,
164 mountain aspen, and elm.

165 Mount Changling ($37^{\circ}12' \sim 37^{\circ}17'$, $102^{\circ}45' \sim 103^{\circ}48'E$) (sampling site henceforth
166 abbreviated as CL) is an independent mountain protruding northward from the
167 remnants of the eastern Qilian Mountains, it is located at the southern edge of the
168 Tengger Desert; its elevations range from 2100 to 2900 m. The dominant tree species
169 are Qinghai spruce and Chinese pine.

170 Mount Dongdashaan ($39^{\circ}00' \sim 39^{\circ}04'N$, $100^{\circ}45' \sim 100^{\circ}51'E$) (sampling site
171 henceforth abbreviated as DS) is located at the southwestern edge of the Badan Jaran
172 Desert and the middle part of Mount Qilian. It is one of the northern mountains along
173 the Hexi Corridor; that range consists of mountains that vary from 2200 to 2637 m in
174 elevation. Forests are dominated by Qinghai spruce and Qilian juniper. The distances
175 between the CL and HL, CL and DS, and DS and HL sampling sites are approximately
176 250 km, 310 km, and 450 km, respectively.

177 The temperatures of the coldest months recorded at meteorological stations in the
178 Alxa Left Banner (a division of the Alxa League region), Jingtai (a county in Gansu),
179 and Zhangye (a city in Gansu) all occurred in January, ranging from $-9.8^{\circ}C$ to $-6.8^{\circ}C$.

180 The hottest months at those stations were in July (21.9 °C to 23.1 °C). These
181 meteorological stations are the closest stations to our three sampling sites (Fig.1).

182 Precipitation measured at those stations varied widely. The multi-year average of
183 total precipitation from May to September was 171 mm at Alxa Left Banner station,
184 156 mm at Jingtai station, and 108 mm at Zhangye station. This accounted for more
185 than 80% of the annual precipitation (Fig.1).

186

187 **2.2 Sample collection, processing and data analysis method**

188 **2.2.1 Sample collection, processing and dendrochronology construction**

189 Researchers used standard methods of tree-ring sample collection. One core was drilled
190 from each tree in the sample site. We collected 209 cores in total, from five sampling
191 sites at HL, 48 cores from one sampling site at CL, and 81 cores from two sampling
192 sites at DS. Relevant information of the sampling sites is summarized in Table 1.

193 Chronologies were constructed using standard dendrochronological methods
194 (Cook, 1985). In order to highlight the high frequency signal, the RES chronology is
195 selected for later climate analysis. We calculated the highly significant correlations (P
196 < 0.001) between the chronologies of different points at the HL and DS mountains; a
197 weighting method was used to finally synthesize a chronology for each mountain.
198 Generally, the sub-sample signal strength (SSS) index and the mean series
199 intercorrelation (R_{bar}) are used to evaluate the credibility and quality of the chronologies.
200 The length of the reliable chronology is indicated by the parts of the series with a
201 subsample signal strength (SSS) index > 0.85 (Wigley et al., 1984). Another important
202 statistic is the mean series intercorrelation (R_{bar}), which is the mean correlation
203 coefficient among the ring series and is therefore an indication of the common variance.

204

205 **2.2.2 Climate data, atmospheric circulation indices and the related Analyzing** 206 **methods for chronological correlation**

207 Climate data for the study areas HL, CL, and DS were collected from the nearest
208 meteorological stations in Alxa Left Banner, Jingtai and Zhangye, respectively
209 (<http://data.cma.cn>).

210 We used SPEI (Standardized Precipitation Evapotranspiration Index) to represent
211 the local drought and wetness conditions, which is widely used in the dendrochronology
212 studies and considering the effects of potential evapotranspiration, precipitation and
213 time scales (Vicente-Serrano et al., 2010). SPEI data (grid-point resolution $0.5^{\circ} \times 0.5^{\circ}$)
214 was obtained from the grid-point datasets of the National Center for Environmental
215 Predictions-National Center for Atmospheric Research (NCEP-NCAR). Time scales
216 ranged from 1 month to 15 months. The mean values of data from two grid-points
217 closest to the HL sampling site (38.75°N , 105.75°E and 38.75°N , 106.25°E ; period
218 1953–2015) were chosen for subsequent analysis. Grid-point data from one site closest
219 to our CL sampling site (37.75°N , 103.75°E ; period 1951–2015) was used for later
220 analysis. Grid-point data from one site closest to our DS sampling site (39.25°N ,
221 100.75°E ; period 1951–2015) was also used. As SPEI datasets are multi-scale, we
222 preprocessed the data to identify and select 11-month scaled SPEI datasets for
223 subsequent analysis.

224 We took into account the so-called lagging effect (the influence of fall and winter
225 climate factors on the radial growth of trees shows up later in the year) and chose to use
226 temperature, precipitation, and SPEI data from September of the previous year to
227 September of the current year (abbreviated as P9–P12 and C1–C9), as collected at each
228 meteorological station, for our climate response analysis.

229 The East Asian Summer Monsoon Index (EASMI) (Li and Zeng 2005) represents
230 the activity strength of the EASM. Larger EASMI values indicate a stronger summer
231 monsoon, smaller ones a weaker monsoon. In this study, the EASMI (mean values for
232 June–August in the period 1950–2017) defined by Li and Zeng (2005) was used to
233 study the impact of the EASM on climate change in the study area.

234 The East Asian Summer Monsoon Index (EASMI) represents the activity strength
235 of the EASM. The East Asian summer monsoon (EASM) index is defined as an area-
236 averaged seasonally (JJA) dynamical normalized seasonality (DNS) at 850 hPa within
237 the East Asian monsoon domain (10° - 40°N , 110° - 140°E) (Li and Zeng 2005). Larger
238 EASMI values indicate a stronger summer monsoon, smaller ones a weaker monsoon.

239 In this study, the EASMI (mean values for June–August in the period 1950–2017)
240 defined by Li and Zeng (2005) was used to study the impact of the EASM on climate
241 change in the study area.

242 We used the Westerly Circulation Index (WCI annual mean; [https://cmdp.ncc-](https://cmdp.ncc-cma.net/cn/index.htm)
243 [cma.net/cn/index.htm](https://cmdp.ncc-cma.net/cn/index.htm)) to represent the strength of the mid-latitude westerlies. The
244 larger the WCI value, the stronger the Eurasian latitudinal circulation; the smaller the
245 value, the weaker the Eurasian latitudinal circulation. WCI data (period 1951–2015)
246 were derived from the Eurasian Latitudinal Circulation Index published by the National
247 Climate Center of the China Meteorological Administration ([https://cmdp.ncc-](https://cmdp.ncc-cma.net/cn/index.htm)
248 [cma.net/cn/index.htm](https://cmdp.ncc-cma.net/cn/index.htm)).

249 Interannual and interdecadal (sliding moving average of 11a) chrono-climatic/
250 cyclonic index correlation and partial correlation analyses were performed using SPSS
251 19.0. Based on the characteristics of tree-ring series, the sequences were classified into
252 three groups of low, average and high ring widths using $\text{mean} \pm 1\delta$ (δ : standard
253 deviation) as the classification criterion (with $\text{mean} \pm 2\delta$ as the extreme year).
254 Correlation statistical tests were performed with the corresponding annual circulation
255 indices; similar treatments and analyses were performed for the two major circulation
256 indices.

257

258 **3. Results and analysis**

259 **3.1 Ring-width chronologies and their characteristics**

260 Based on the sampling cores from five sample sites at HL, two sample sites at DS, and
261 one sample site at CL, ring-width residual chronologies were derived for each of the
262 three study areas (Fig. 2). Statistical parameters showed that the three chronologies
263 meet the usual requirements for correctly done dendrochronological studies (Table 1).
264 Table 1. Statistical characteristics of the sampling sites and the tree-ring chronologies.

265

266 Table 1. Statistical characteristics of the sampling sites and the tree-ring chronologies.

Sampling sites	HL(5)	CL(1)	DS(2)
Latitude (°N)	38.52–38.97	37.61	39.04

Longitude (°E)	105.83–106.02	103.71	100.78
Elevation (m)	2200–2750	2490	2650–2700
Cores	209	48	81
Reliable period	1891–2018	1866–2017	1823–2015
MS	0.18–0.37	0.28	0.15–0.33
R_{bar}	0.45–0.61	0.56	0.40–0.60
SNR	22.5–56.1	38.9	25.7–42.5
EPS	0.96–0.98	0.98	0.96–0.98
PC1(%)	17.3–63.0	57.9	43.0–62.5

267 Reliable period (SSS > 0.85), MS (mean sensitivity), R_{bar} (mean series intercorrelation), SNR (signal to
 268 noise ratio), EPS (expressed population signal), and PC1 (variance explained by the first principal
 269 component) refer to residual chronologies).

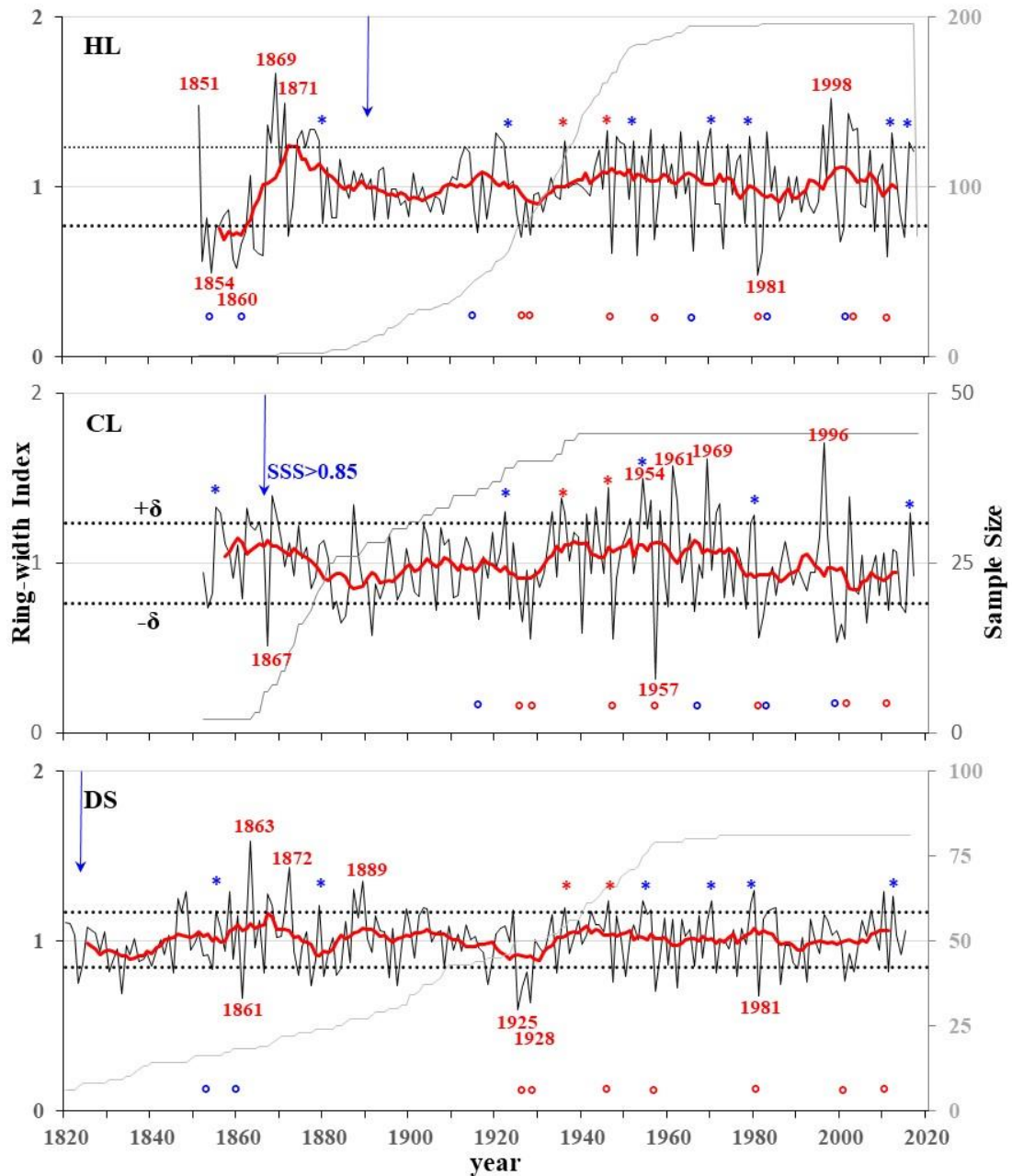
270

271 **3.2 Climate response characteristics**

272 Correlation analysis comparing a) monthly mean temperature and precipitation at
 273 neighboring meteorological stations and b) SPEI at the nearest grid-point showed that,
 274 overall, the three residual chronologies were correlated negatively with monthly mean
 275 air temperature, positively correlated with monthly precipitation, and positively
 276 correlated with SPEI during the growing season (Fig. 3).

277 HL chronology was correlated negatively with mean temperature mainly in C5–C8
 278 in the growing season, but not to the significant level. It was also positively correlated
 279 with precipitation in all months except P12, C1, and C9, reaching significant levels (P
 280 < 0.05) in P9, C5, and C6. All months were positively correlated with SPEI and reached
 281 statistical significance (P < 0.05), with C3–C8 showing highly significant correlation
 282 levels (P < 0.01).

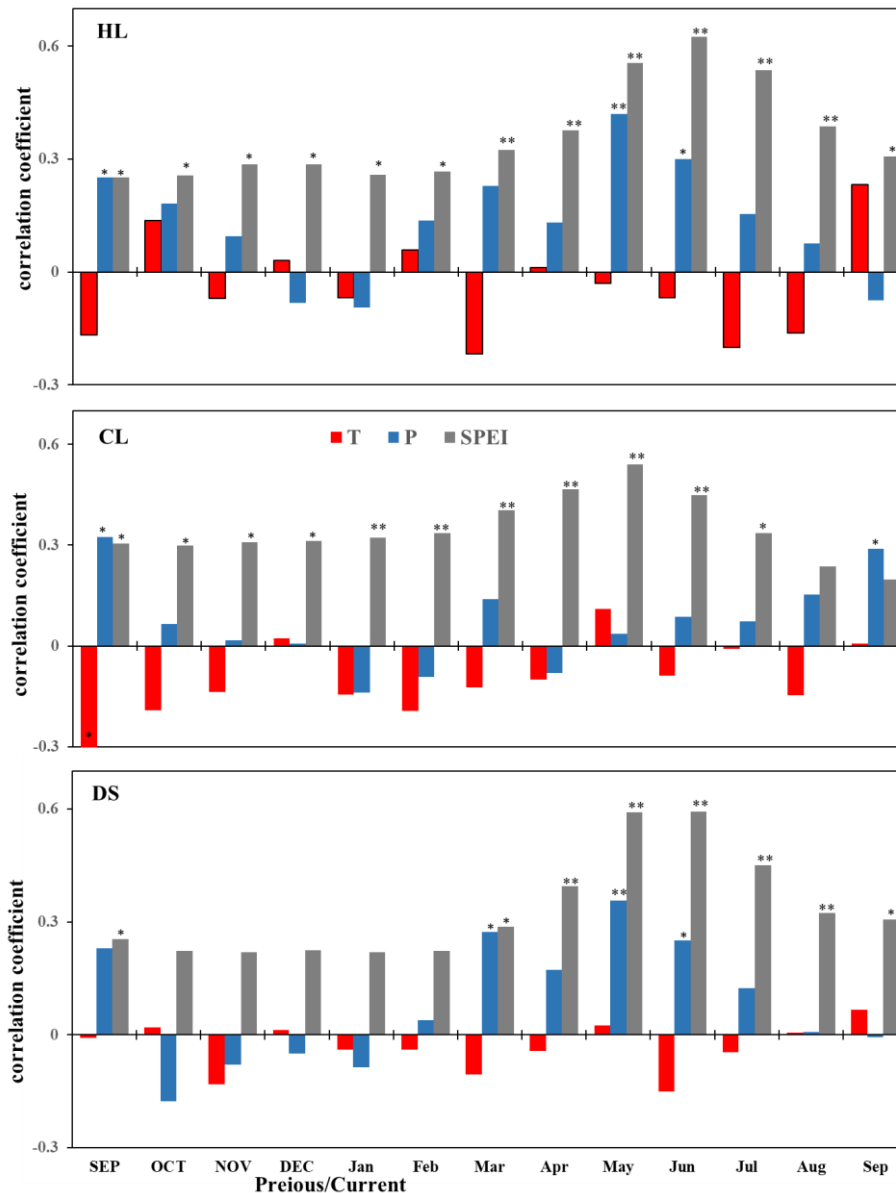
283



284

285 **Figure 2.** Residual ring-width chronologies for the three study areas. The dark lines indicate the
 286 chronology; grey lines indicate the sample depth; red lines indicate the 11-year running mean
 287 chronology; dotted horizontal lines indicate the mean value $\pm 1\delta$; years with data identified as $>/<$
 288 mean $\pm 2\delta$ (δ : standard deviation); blue * and o indicate the years shared between two of the three
 289 sample sites, red * and o shows years shared between three sample sites; blue arrows indicate the
 290 start of the reliable residual chronology ($SSS > 0.85$).

291



292

293 **Figure 3.** Correlation coefficients (Pearson's r values) between the residual ring-width chronologies

294 of Qinghai spruce at the three study areas (HL, CL and DS) and the observed monthly temperature

295 (T), total monthly precipitation (P), and SPEI. * Pearson's r correlation, significant at $P < 0.05$. **

296 Pearson's r correlation, significant at $P < 0.01$. Month names of previous year are capitalized.

297

298 CL chronology was negatively correlated with the mean temperature in most

299 months, but only reached a significant negative correlation ($P < 0.05$) with P9. CL

300 chronology was positively correlated with monthly precipitation, save for C1, C2, and

301 C4. Only P9 and C9 reached statistical significance ($P < 0.05$). All months were

302 positively correlated with SPEI, with P9–C7 reaching significant correlation levels (P
303 < 0.05) and C1–C7 reaching highly significant correlation levels ($P < 0.01$).

304 DS chronology showed weak correlations between DS chronology and monthly
305 mean temperatures. None of the correlations reached levels of significance. DS
306 chronology was positively correlated with P9 and C2–C8 precipitation and reached
307 significant correlation levels for C3, C5, and C6 ($P < 0.05$). All months were positively
308 correlated with SPEI, with P9 and C3–C9 reaching significant correlation levels ($P <$
309 0.05) and C4–C8 reaching highly significant correlation levels ($P < 0.01$).

310 Overall, the radial growth of Qinghai spruce at the three study areas seems to have
311 been limited, for the most part, by low precipitation during the growing season (April–
312 July). The three chronologies reflect regional wet and dry variations.

313

314 **3.3 Regional climate changes as recorded by tree-ring widths**

315 **3.3.1 Regional climate change viewed at interannual scales**

316 On interannual scales, the three residual chronologies, when compare, showed highly
317 significant correlations (HL–CL: $n = 166$, $r = 0.298$, $P < 0.001$; HL–DS: $n=165$, $r=0.331$,
318 $P < 0.001$; CL–DS: $n = 164$, $r = 0.374$, $P < 0.001$). This indicates that there was a high
319 degree of consistency in the radial growth of Qinghai spruce in the three regions.

320 According to the results of the chronology-climate response analysis in the
321 previous section, the high and low ring-width indices ($\text{mean} \pm 1\sim 2\delta$) of the chronology
322 at the three sample sites indicate wetter or drier, and extreme wet or dry years,
323 respectively (Fig. 2).

324 Overall, the three ring-width residual chronologies (HL, CL, DS) had a total of two
325 shared wetter years and seven shared drier years. The HL and CL chronologies shared
326 four wet years and eleven dry years; the HL and DS chronologies shared five wet years
327 and nine dry years; and the CL and DS chronologies shared five wet years and seven
328 dry years (Fig. 2).

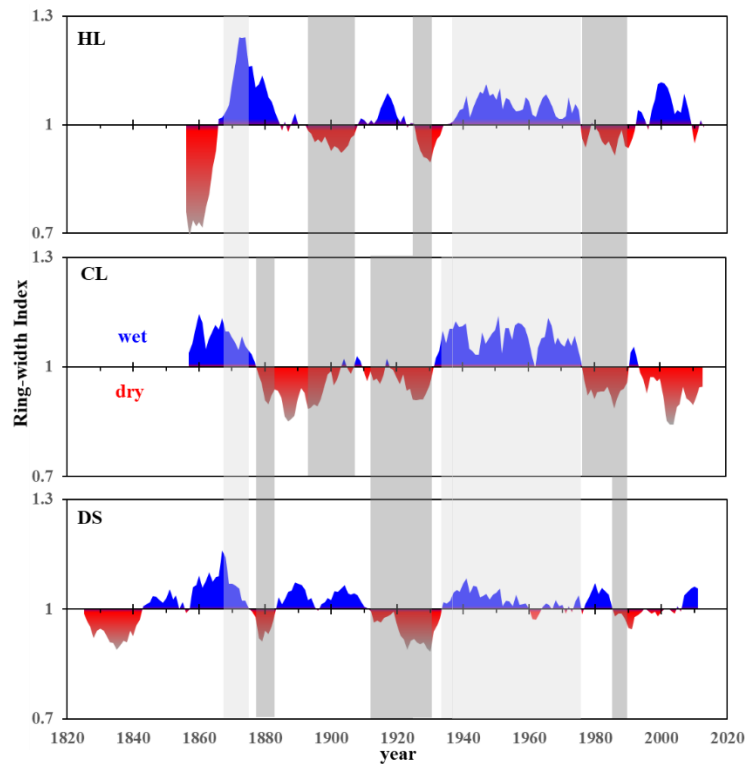
329 There were no extremely wet years shared by the three sample sites. However, there
330 were two shared wetter years in 1936 and 1946 and several shared wetter years in later
331 years among the three sample sites. For example, note the wetter years in 1922 and
332 2016 for HL and DS chronologies; 1959, 1979, and 2012 for HL and DS chronologies;
333 1855, 1954, and 1980 for CL and DS chronologies (Fig. 2).

334 The extreme drought years are consistent among the three sample sites. For
335 instance, there was an extreme drought year in 1981 at HL and DS sample sites; it was
336 also a drought year at CL. An extreme drought year at CL in 1957 was also a drought
337 year for the other two chronologies. Moreover, the extreme drought year of 1928 at DS
338 was a drought year at the other two sites. Drought years in 1926, 1947, 2001, and 2011
339 were seen in all three sites and in two of the three sample sites (1916, 1966, 1982, and
340 2000 at HL and CL; 1854 and 1861 at HL and DS) (Fig. 2).

341

342 **3.3.2 Characteristics of regional climate change at inter-decadal scales**

343 On the decadal scale, the 11a running mean series indicates that at the HL site there
344 were four wetter periods (mid-1860s to early 1880s; 1910s to 1920s; mid-1930s to mid-
345 1970s; and late 1990s to early 2010s). Four drought periods were seen (mid-1850s to
346 mid-1860s; early 1890s to late 1900s; circa 1930s; and mid-1970s to 1980s) (Fig.4).



347

348 **Figure 4.** Three regional chronologies demonstrating alternation between dry (red) and wet (blue)
 349 years on interdecadal scales (11 a running mean). The gray and light gray bands indicate consistent
 350 changes of the dry and wet periods.

351

352 The CL regional chronology revealed two main wetter periods (mid-1850s to mid-
 353 1870s; mid-1930s to mid-1970s) and two longer drought periods (late 1870s to early
 354 1930s; following the late 1970s) (**Fig.4**).

355 The DS regional chronology showed four main wetter periods (mid-1840s to mid-
 356 1870s; mid-1880s to late 1900s; mid-1930s to mid-1980s; and late 2000s to early
 357 2010s). There were four drought periods (mid-1820s to mid-1840s; mid-1870s to 1880s;
 358 early 1910s to early 1930s; and late 1980s to mid-2000s). The drought during the last
 359 drought period was less severe (**Fig.4**).

360 The three chronologies show both synchronized phases and differential changes on
 361 an interdecadal scale. The more synchronized dry phases of climate change were the
 362 drought periods of the 1930s and 1990s. When we compared the DS chronology to the
 363 HL and CL chronologies on decadal scales, we noted that DS droughts tended to last

364 longer and that they started and ended later than CL droughts. However, HL and DS
365 droughts tended to end at the same time (Fig.4).

366 There were two wet periods in 1870s and the mid-1930s to 1970s which were
367 shared by all three sample sites. The latter period was the longest lasting wet period we
368 saw in our study. There were also dry and wet periods that were not shared by any of
369 our sites. There was an HL drought (mid-1850s to mid-1860s) which was not shared by
370 the other two sites, which were wetter. HL and CL shared drought periods (1890s to
371 1910s; 1980s) while DS was wetter. Conversely wetter periods at HL were sometimes
372 accompanied by drought in the other two sites. Drought at CL was sometimes
373 accompanied by wet periods at the other two sites. DS was wet during the 2010s but
374 the other two sites were in drought (Fig.4).

375 The results of the above studies show that there are diversified and complex
376 features in the interdecadal processes of climate change in different regions around the
377 Alxa Plateau.

378

379 **3.4 Driving mechanism of the regional climate changes**

380 **3.4.1 Driving mechanism of the regional climate changes of typical years**

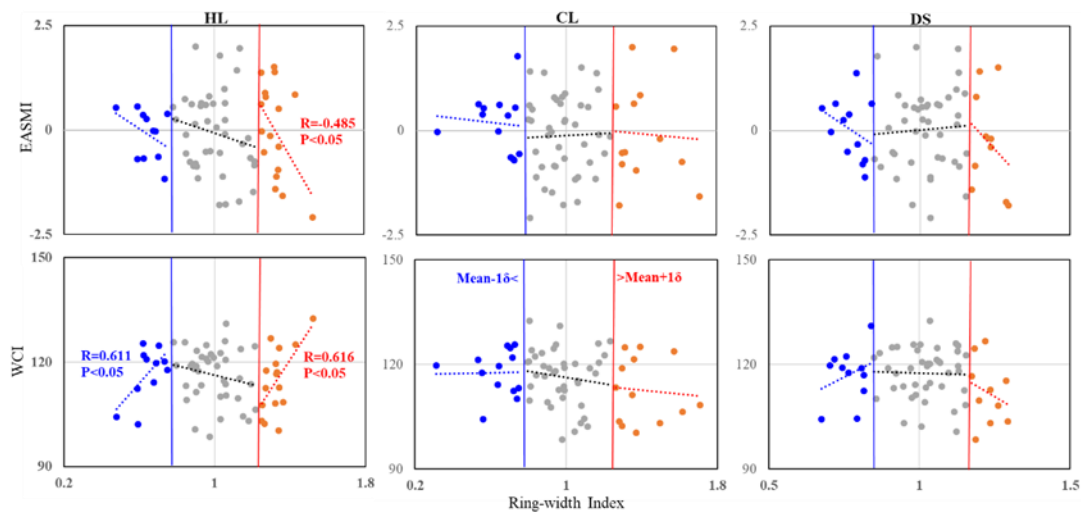
381 On the interannual scales, three regional chronologies we developed showed fairly
382 weak negative correlations between the EASM and the westerlies; none of the
383 correlations were statistically significant. We carried out correlation analyses of the
384 three regional ring-width chronologies and two major circulation indices. This was
385 done in high, medium and low ring-width index groups (Fig. 5; 6).

386 At HL, the results of our combined subgroup correlation analyses suggest that
387 correlations between radial growth groups and atmospheric circulations were stable.
388 Correlation between the higher ring-width group and atmosphere circulation indices
389 and between the lower ring-width group and the WCI were all significant ($P < 0.05$)
390 (Fig. 5; 6).

391 At CL, correlations between the higher and middle ring-width groups to the WCI
392 and the higher and middle WCI groups to the ring-width index were all negative.
393 Correlations between the higher and middle ring-width groups and the EASMI, and

394 between the higher and middle EASMI groups with the ring-width index were
 395 inconsistent (Fig. 5; 6).

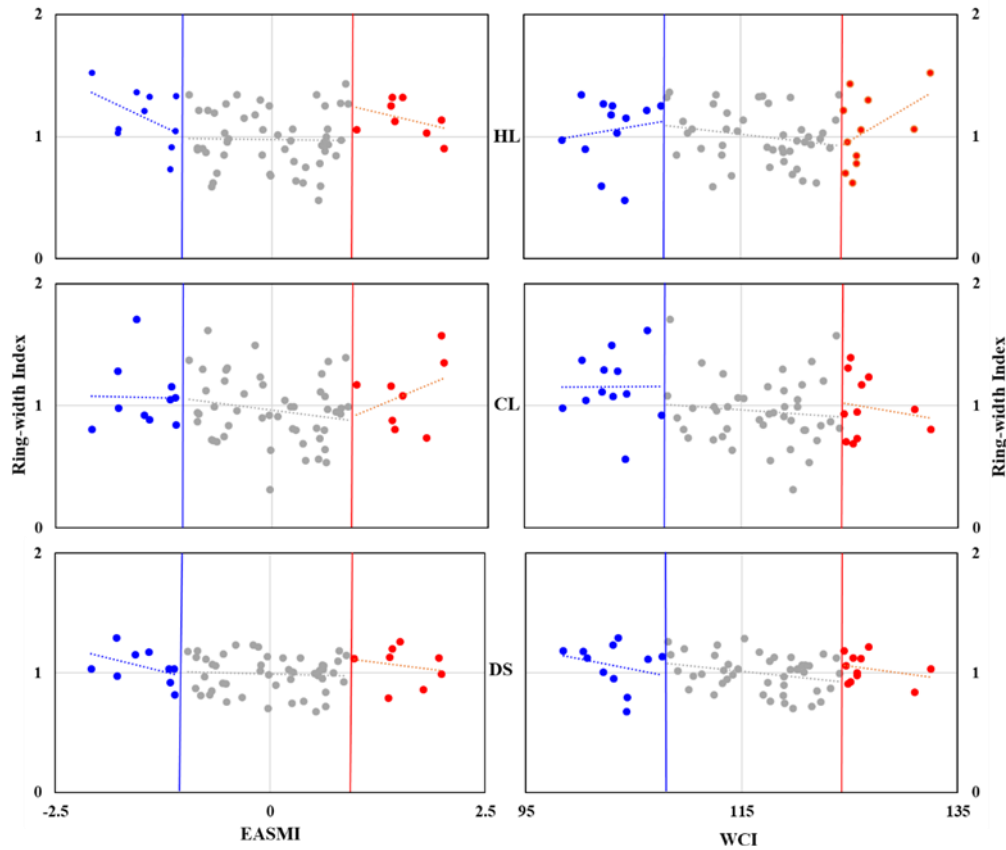
396 At DS, correlations between the higher and lower ring-width groups and the
 397 EASMI, and between the higher and lower EASMI groups to the ring-width indices,
 398 were consistent. The correlations between the higher ring-width groups and the WCI,
 399 and between the higher WCI groups and the ring-width index were consistent. However,
 400 the correlations between the lower ring-width groups and the WCI, also between the
 401 lower WCI groups and the ring-width index, were inconsistent (Fig. 5; 6).



402
 403 **Figure 5.** Grouping related charts among the ring-width index of three regions (HL, CL and
 404 DS) and the two atmospheric circulations' indices (EASMI and WCI), grouped by chronological
 405 values. The noted numbers are the person correlation coefficients (two-tails test) and the
 406 corresponding significant credible level. Only the significant correlations were labeled. Red dots
 407 indicate the higher ring-width index group ($> \text{mean}+1\delta$), gray dots indicate the middle ring-width
 408 index group ($> \text{mean}-1\delta \sim < \text{mean}+1\delta$), and blue dots indicate the lower ring-width index group ($>$
 409 $\text{mean}-1\delta$).

410
 411 Except for HL, none of the ring-width groups or the atmospheric circulation index
 412 groups of the others reached a level of significance. These results suggest that HL is
 413 strongly affected by size of, and the interaction between, the EASM and the Westerly
 414 winds. On an interannual scale, stronger west winds and a weaker monsoon could result
 415 in variations from the ordinary climate (veering towards drier or wetter). Weaker west

416 winds and a stronger monsoon formed the normal climate at HL. At the CL and DS
 417 sites, both atmospheric circulations were relatively weak on interannual scales. They
 418 had complex interactions.



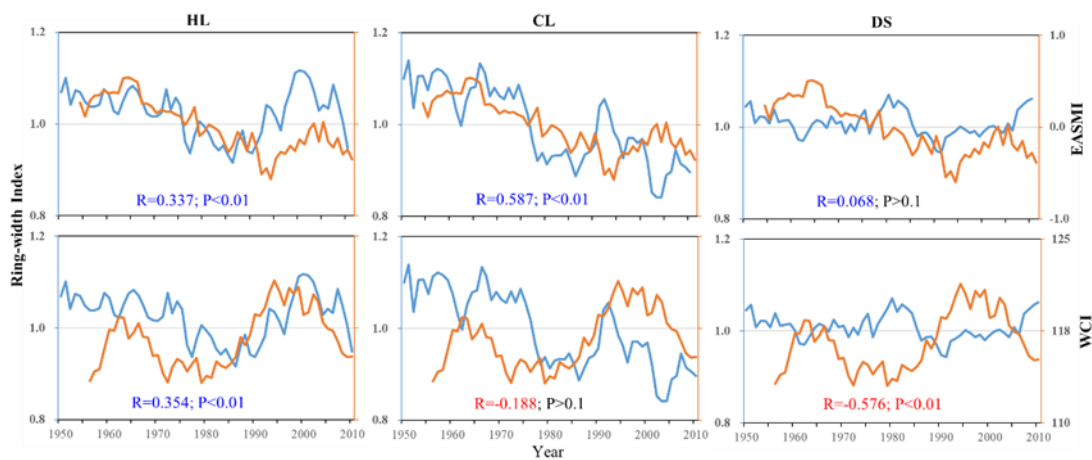
419
 420 **Figure 6.** Grouping related charts among the two atmosphere circulations' index (EASMI and WCI)
 421 and the ring-width index of three regions (HL, CL, and DS), grouped by the two atmosphere
 422 circulations' index. Red dots indicate the higher atmosphere circulations' index group ($> \text{mean} + 1\delta$),
 423 gray dots indicate the middle atmosphere circulations' index group ($> \text{mean} - 1\delta \sim < \text{mean} + 1\delta$), and
 424 blue dots indicate the lower atmosphere circulations' index group ($> \text{mean} - 1\delta$).

425

426 **3.4.2 Driving mechanisms of the regional climate changes on a decadal scale**

427 At HL, both the EASM and the westerly circulation had highly significant effects on
 428 the radial growth of the Qinghai spruce. At CL, the EASM also had highly significant
 429 effects on radial growth of the Qinghai spruce. There, correlation coefficients were
 430 higher for the EASMI (EASM index) than they were for the HL index. Correlations
 431 between the WCI and radial growth were negative, but not at a significant level.

432 At DS, correlation between radial growth and the WCI was extremely negative (P
 433 < 0.01). Correlation between radial growth and the EASM was positive ($P > 0.1$) (Fig.
 434 7). These results suggest that at HL, alternations between dry and wet seasons were
 435 affected both by the EASM and the westerlies. If either of the two atmospheric
 436 circulations was stronger, the climate tended to be wetter. At CL, alternations between
 437 dry and wet were affected mainly by the EASM. When the EASM was stronger, the
 438 climate was wetter. At DS, the climate was affected mainly by the westerlies. The
 439 stronger the winds, the wetter the climate (Fig. 7).



440

441 **Figure 7.** Interdecadal scale (11-a running average) correlations of the three residual chronologies
 442 with the EASMI and WCI.

443

444 The results of our interdecadal partial correlation analysis of the three RES-
 445 chronologies with the WCI and EASMI further illustrate the impacts of the two
 446 circulation systems on the climate of the three regions (Table 2).

447 At HL, if we control one variable (the WCI or EASMI) from our analysis, the other
 448 variable will all showed a positive correlation with its chronology ($P < 0.0001$). At CL,
 449 if we controlled the WCI, we find a positive significant correction between the
 450 chronology and EASMI ($P < 0.0001$). If we controlled the effect of EASMI, we saw a
 451 weak negative correction between the chronology and WCI (Table 2). At DS, if we
 452 controlled EASMI, we saw a negative significant correlation between the chronology
 453 and WCI ($P < 0.0001$). If we controlled the WCI, we saw an insignificant negative
 454 correlation between the chronology and EASMI (Table 2).

455 Table 2. Inter-decadal partial correlation analysis of the three residual-chronologies
 456 with the WCI and EASMI.

	HL	CL	DS
WCI	0.489 ***	0.550***	-0.172
EASMI	0.511***	-0.001	-0.591***

457 Correlation significance levels (two-tailed test): *** P < 0.001.

458 Summary: at HL (on the eastern boundary of the Alxa Plateau), both EASMI and
 459 WCI influenced the alternation between wet and dry; at CL (on the southern boundary
 460 of the Alxa Plateau), climate was mainly influenced by the EASM. At DS (on the
 461 western boundary of the Alxa Plateau and the middle part of Hexi Corridor), climate
 462 was mainly influenced by the westerlies.

463

464 **4. Discussion and conclusions**

465 **4.1 Climate changes indicated by regional chronologies**

466 Our chronology-climate response analysis (Fig. 3) showed that the radial growth index
 467 of Qinghai spruce in the HL, CL and DS mountains were a good record of regional
 468 climate changes around the Alxa Plateau (Fig. 2). On the interannual scale, the three
 469 regional chronologies noted that the extreme drought years of 1928, 1957 and 1981
 470 were shared by two or more locations, as were the drought years of 1854, 1861, 1916,
 471 1926, 1947, 1966, and 2001 (Fig. 2).

472 We note that drought was also reported by other tree-ring studies for these regions
 473 (Chen et al., 2016), also for the Qilian Mountains (Zhang et al., 2011; Zhang et al.,
 474 2017). Several other drought years (1854, 1884, and 1925–1928) were also seen in the
 475 dry-wet climate history (PDSI and recorded by tree-ring-widths) in the nearby area of
 476 Mount Hasi, which lies on the edge of the regions most influenced by the EASM (Kang
 477 et al., 2012).

478 The drought years of 1823, 1833, 1854, 1877, 1883–1885, 1895, 1908, 1971, 1992,
 479 and 2003 seen in results for the Alxa Plateau are also seen in twelve tree-ring
 480 reconstructed drought series for the Qilian Mountains (an area mainly influenced by
 481 westerlies) (Zhang et al., 2011). We also note that wetter years seen in our three regional

482 chronologies were also seen in results from the Hasi and Xinglong Mountains, which
483 are also on the edge of the area influenced by the EASM) (Fang et al., 2009; Kang et
484 al., 2012).

485 If we compare our results with those seen for the EASM-affected areas at Mount
486 Guiqing, 1820–2005 (Fang et al., 2010), we noted that only three of the eight drought
487 years in that area (1928, 2000, and 2001) were seen in our three chronologies. We also
488 noted results from the westerly-influenced area at Mount Tianshan (Jiang et al., 2017).
489 The wetter years of 1846, 1903 and 1942 at DS were also extreme wet years at Mount
490 Tianshan. Two wet years, 1848 and 1959, recorded at DS are either one year earlier or
491 one year later than extremely wet years at Mount Tianshan, which might suggest some
492 correlation. Drier years at DS (1884, 1947 and 1951) are one or two years later than the
493 extremely dry years at Mount Tianshan. This suggests that these phenomena could be
494 related to broader changes in the extent and strength of the atmospheric circulation.

495 On a broader (interdecadal) scale, an extreme drought period in 1920s–1930s was
496 shared by much of northern China (Liang et al., 2006; Fang et al., 2009; Fang et al.,
497 2010). This is the same drought that we note our chronologies for HL, CL and DS (Liu
498 et al., 2002; Chen et al., 2010; Fan et al., 2012; Liu et al., 2013; Zhang et al., 2015). A
499 drought in 1890–1900 was noted by dendrochronological studies and regional history
500 documents (Yuan, 1994; Ma et al., 2003; Cai and Liu, 2007).

501 Ma and Fu's (2006) study showed a broad shift towards a drying climate in 1977–
502 78 (eastern area in northwestern China, also northern China). Several other
503 dendrochronological studies showed a combination of high temperatures and low
504 precipitation in the late 1970s to early 1990s (Zhang et al., 2005b; Cai and Liu, 2007;
505 Cai, 2009). This same drought was seen at DS, if somewhat later and for a shorter time.
506 We also noted its effects at HL and CL. This would be consistent with the increased
507 humidity of the climate in the eastern region of Northwest China (the EASM-influenced
508 region experiencing > 400 mm precipitation). This region would include Mount
509 Xinglong (Fang et al., 2009; Chen et al. 2015), the easternmost part of the Qilian
510 Mountains, and Mount Guiqing (Fang et al., 2010).

511 The wet period that lasted from the 1940s to the early 1970s has been recorded by
512 several tree-ring-width chronologies covering HL, CL, and DS (Liu et al., 2004; Liu et
513 al., 2005; Gao et al., 2006; Cai, 2009; Chen et al., 2010). Regional history documents
514 also record some severe floods disasters in this period (Yuan, 1994). We also see this
515 wet period in tree-ring-width chronologies from Mount Xinglong (Fang et al., 2009;
516 Chen et al. 2015) and Mount Guiqing (Fang et al., 2010).

517 The wet period in the 1830s–1840s evident in the chronologies in Xinglong
518 Mountain (Fang et al., 2009) (Chen et al. 2015) and Guiqing Mountain (Fang et al.,
519 2010) corresponds to the dry period of DS. The wet period in the 1830s–1840s
520 corresponds to the dry period of HL and CL, and to the wet period of DS. The observed
521 phenomena can be attributed to differences in the extent and intensity of EASM and
522 westerly atmospheric circulations.

523

524 **4.2 Influence of atmospheric circulations and their interaction on climate change** 525 **in the Alxa Plateau**

526 Water vapor carried by the westerlies will extend southward to the northern part of
527 Qinghai, the Hexi region of Gansu, the northern part of Ningxia, and the northern part
528 of Shaanxi Province, sometimes passing through the northern border of the Xinjiang
529 region (Li et al., 2012). The area bounded by 35° and 55°N, and 110°E and 140°E seems
530 to be crucial to fluctuations in the westerlies. This in turn affects the distribution of rain
531 belts in summer. Its mean WCI are weaker positively to the rainfall in the middle of
532 Yellow River Basin and its northern regions (Yan et al., 2007). The results showed that
533 the middle ring-width index group of Qinghai spruce in the three sample sites, which
534 are located in the key area for interaction between wind and monsoon, presented weaker
535 negative correlation with WCI on the interannual scale (Fig. 5).

536 The EASM boundary zone has a greater influence on precipitation at higher
537 latitudes and thus on vegetation growth. This boundary zone can fluctuate due to the
538 interannual variability of the EASM and the westerlies. There may be lagging effects
539 at the mid-latitudes (Ou and Qian, 2006). Again, we note that on an interannual scale,

540 there is much variation in the strengths and interactions of the EASM and westerly
541 circulation and thus on climate in our three study regions (Fig. 5).

542 Sun et al. (2019) showed that when the westerly circulation strengthens, high
543 latitude air pressure drops across the entire Asian continent. Siberian high pressures and
544 the EASM are weakened. The southward movement of the cold air is also
545 correspondingly weakened. That is not conducive to the north and south of the cold and
546 warm air vapor exchange to form precipitation. When the lower of the WCI and
547 weakened latitudinal circulation, the meridional circulation will strengthen, which
548 favors the exchange of warm and cold air between the north and south to form
549 precipitation.

550 Yang et al. (2019) proposed that in years with weak summer westerlies in the
551 middle latitudes, the upper-level jet stream tends to shift southward. This southward
552 displacement of the jet stream, coupled with weakened lower-level divergence, hampers
553 the northward transport of warm air into the southwestern region. Consequently, this
554 leads to reduced availability of water vapor sources and ultimately results in diminished
555 summer precipitation within the transitional zone of typical monsoon activity. If the jet
556 stream moves northward, precipitation increases.

557 Xu et al. (2010) indicated that in the middle Qilian Mountains the westerlies affect
558 precipitation directly, while the EASM only indirectly affects precipitation. When the
559 westerlies become stronger (weaker), the high precipitation zone moves northwestward
560 (southeastward).

561 At DS, radial growth showed weak negative correlations with higher WCI and also
562 higher, middle, and lower EASMI groups (Figs. 5; 6). At HL, when high chronology
563 indices are positive they are significantly correlated with westerly circulation; when
564 they are negative they significantly correlate with EASM (Figs. 5; 6). At CL, which lies
565 further to the south than HL, a higher EASMI leads to a more humid climate. Other
566 effects are more complicated: for example, the higher and lower ring-width index
567 groups, associated with extreme dry and wet climate years, have weak negative
568 correlations to EASMI (Figs. 5; 6). Jiang et al. (2019) published the results of their
569 hydrogen and oxygen isotope studies of surface water at more than 3,000 sampling sites

570 in northern China. They showed that surface water recharge in the DS Mountains is due
571 to the westerlies; recharge in the CL Mountains is due to the EASM. The HL Mountains,
572 in contrast, sit at the boundary of the EASM; water recharge there is due to both the
573 EASM and the westerlies.

574 Jiang and Wang (2005) notes significant declines in the EASM in the mid-1960s
575 and mid-1970s, which led to decline in the radial growth of Qinghai spruce in our study
576 area. The effect of the latter declined period was much greater than that of the former,
577 whatever the intensity or duration. The effects of these declines were stronger at CL
578 and DS than at HL. In the mid-1970s, EASM retreat had stronger negative effects at
579 CL and then at HL. However, decline in the EASM proved to be a facilitator of radial
580 growth at DS (Fig. 7).

581 In the same period the westerly circulation also retreated. The EASM retreated
582 again in 1990s, while the westerlies strengthened. This resulted in a drier climate in the
583 CL Mountains. However, it was also correlated with fluctuating wet periods at HL and
584 a weak wet period at DS. The above results, to a certain extent, support our view on the
585 driving mechanisms of climate change in the three study areas, especially in the DS
586 Mountains.

587 When we look at this area on a geologic scale, we learn that the westerly circulation
588 strengthened during the Ice Age. Westerly jet streams moved southward to about 35°N.
589 When the westerlies weakened in the Interglacial Age, the westerly jet streams moved
590 northward to ~37°N (Sun et al., 2003). A study of Holocene lake level evolution in the
591 ancient Zhuye lake, central Alxa Plateau, showed that lake-level change was subject to
592 the combined effects of EASM and the arid climate of Central Asia (Li, 2009). This
593 result further illustrates the complexity of lake evolution and climate change in the
594 EASM marginal zone.

595 The westerly circulation also interacts with the monsoon on the Tibetan Plateau,
596 which has a profound effect on the climate of the Asian monsoon region as well as the
597 global climate (Qu et al., 2004). There has also been much research using proxy
598 indicator cycles indicating that our study area is also influenced by large-scale ocean-
599 atmosphere changes on interannual and interdecadal scales, such as the North Atlantic

600 Oscillation (NAO), Pacific Decadal Oscillation (PDO), El Niño-Southern Oscillation
601 (ENSO), and sunspot activity (Gou et al., 2015a; 2015b; Liu et al., 2016; Wang et al.,
602 2017). Generally, the intensity of ENSO was inversely correlated with the intensity of
603 the EASM. There was a negative correlation between PDO and regional dry-wet
604 variation in the west of 100° E. When the NAO is in positive phase (negative phase), it
605 indicates that the mid-latitude westerly winds are in strong (declining) phase, which is
606 conducive to (unfavorable) precipitation formation.

607 However, all of the above-mentioned large-scale climate and ocean-atmosphere
608 changes affect the EASM and westerly circulation through different pathways (Li.
609 2009), which in turn have various effects on the northwestern edge zone of the EASM
610 and the zone of interaction between the two major atmospheric circulations.

611 In conclusion, based on the analysis of the regional chronologies collected in the
612 HL, CL and DS mountains that are arrayed around the Alxa Plateau, we can safely assert
613 that the radial growth of Qinghai spruce in the study area is mainly affected by regional
614 precipitation. This precipitation varies constantly over time and space, primarily
615 influenced by the interactions between two atmospheric circulation systems, EASM
616 and westerlies. At HL, both of these atmospheric circulation systems play a significant
617 role in shaping climate changes. At CL, the climate is mainly influenced by the EASM.
618 At DS, climate is more heavily influenced by the westerly circulation.

619 In the future, it is to be hoped that more refined, smaller scale research can be done
620 on the climate history in the deserts of the Alxa Plateau. Such research may finally to
621 provide a theoretical basis to explain regional climate driving mechanisms and thus
622 enable better desertification controls.

623

624 **Acknowledgements**

625 The study was jointly funded by the National Natural Science Foundation of China
626 (NSFC) (No.42171031; 42171167); Inner Mongolia Autonomous Region Special Fund
627 project for transformation of Scientific and technological Achievements (2021CG0046).

628

629

630 **References**

- 631 Cai, Q. F.: Response of *Pinus tabulaeformis* tree-ring growth to three moisture indices and
632 January to July Walter index reconstruction in Helan mountain, Marine geology &
633 Quaternary geology, 29, 131–136 (In Chinese with English abstract),
634 <https://doi.org/10.3724/SP.J.1140.2009.06131>, 2009.
- 635 Cai, Q. F. and Liu, Y.: January to August temperature variability since 1776 inferred from tree-
636 ring width of *Pinus tabulaeformis* in Helan Mountain, Journal of Geographical Sciences,
637 17, 293–303, <https://doi.org/10.1007/s11442-007-0293-5>, 2007.
- 638 Chen, F., Yuan, Y. J., Zhang, T. W., and Linderholm, H. W.: Annual precipitation variation for
639 the southern edge of the Gobi Desert (China) inferred from tree rings: linkages to climatic
640 warming of twentieth century, Nat. Hazards, 81, 939–955, [https://doi.org/10.1007/s11069-](https://doi.org/10.1007/s11069-015-2113-z)
641 015-2113-z, 2016.
- 642 Chen, F., Wei, W. S., Yuan, Y. J., Yu, S. L., Shang, H. M., Zhang, T. W., Zhang, R. B., Wang, H.
643 Q., and Qin, L.: Variation of annual precipitation during 1768–2006 in Gansu Inferred from
644 multi-site tree-ring chronologies, Journal of Desert Research, 33, 1520–1526 (In Chinese
645 with English abstract), <https://doi.org/10.7522/j.issn.1000-694X.2013.00218>., 2013.
- 646 Chen, F., Yuan, Y. J., Wei, W. S., Yu, S. L., Fan, Z. A., Zhang, R. B., Zhang, T. W., Li, Q., and
647 Shang, H. M.: Temperature reconstruction from tree-ring maximum latewood density of
648 Qinghai spruce in middle Hexi Corridor, China, Theoretical and Applied Climatology, 107,
649 633–643, <https://doi.org/10.1007/s00704-011-0512-y>, 2012.
- 650 Chen, F., Yuan, Y. J., Wei, W. S., Yu, S. L., Li, Y., Zhang, R., Fan, Z., Zhang, T., and Shang, H.:
651 PDSI changes of May to July recorded by tree rings in the northern Helan Mountains,
652 Advance in Climate Changes Research, 65, 344–348 (In Chinese with English abstract),
653 2010.
- 654 Chen, F. H., Chen, J. H., Huang, W., Chen, S. Q., Huang, X. Z., Jin, L. Y., Jia, J., Zhang, X. J.,
655 An, C., and Zhang, J.: Westerlies Asia and monsoonal Asia: spatiotemporal differences in
656 climate change and possible mechanisms on decadal to sub-orbital timescales, Earth-Sci.
657 Rev., 192, 337–354, <https://doi.org/10.1016/j.earscirev.2019.03.005>, 2019a.
- 658 Chen, F. H., Fu, B. J., Xia, J., Wu, D., Wu, S. H., Zhang, Y. L., Sun, H., Liu, Y., Fang, X. M.,
659 Qin, B. Q., Li, X., Zhang, T. J., Liu, B. Y., Dong, Z. B., Hou, S. G., Tian, L. D., Xu, B. Q.,
660 Dong, G. H., Zheng, J. Y., Yang, W., Wang, X., Li, Z. J., Wang, F., Hu, Z. B., Wang, J.,
661 Liu, J. B., Chen, J. H., Huang, W., Hou, J. Z., Cai, Q. F., Long, H., Jiang, M., Hu, Y. X.,
662 Feng, X. M., Mo, X. G., Yang, X. Y., Zhang, D. J., Wang, X. H., Yin, Y. H., and Liu, X.
663 C.: Major advances in studies of the physical geography and living environment of China
664 during the past 70 years and future prospects, Science China Earth Sciences, 62, 1665–
665 1701, <https://doi.org/10.1007/s11430-019-9522-7>, 2019b.
- 666 Chen, J., Huang, W., Jin, L., Chen, J. H., Chen, S. Q., and Chen, F. H.: A climatological northern
667 boundary index for the East Asian summer monsoon and its interannual variability,
668 Science China Earth Sciences, 61, 13–22, <https://doi.org/10.1007/s11430-017-9122-x>,

- 669 2018.
- 670 Cook E.R.: A Time Series Analysis approach to tree ring standardization (Dendrochronology,
671 forestry, dendroclimatology, autoregressive process)[D]. Tuscon, Arizona: The University
672 of Arizona, 1985.
- 673 Ding, Y. H., Liu, Y. J., Xu, Y., Wu, P., Xue, T., Wang, J., Shi, Y., Zhang, Y. X., Song, Y. F., and
674 Wang, P. L.: Regional responses to global climate change: progress and prospects for trend,
675 causes, and projection of climatic warming-wetting in Northwest China, *Advances in*
676 *Earth Science*, 38, 551–562 (In Chinese with English abstract),
677 <https://doi.org/10.11867/j.issn.1001-8166.2023.027>, 2023.
- 678 Fan, Z. A., Wei, W. S., Chen, F., and Yuan, Y. J.: Precipitation variation from 1775 to 2005 at
679 the eastern margin of Tengger Desert, China inferred from tree-ring, *Journal of Desert*
680 *Research*, 32, 996–1002 (In Chinese with English abstract), 2012.
- 681 Fang, K. Y., Gou, X. H., Chen, F. H., D'arrigo, R., and Li, J. B.: Tree-ring based drought
682 reconstruction for the Guiqing Mountain (China): linkages to the Indian and Pacific
683 Oceans, *Int. J. Climatol.*, 30, 1137–1145, <https://doi.org/10.1002/joc.1974>, 2010.
- 684 Fang, K. Y., Gou, X. H., Chen, F. H., Yang, M. X., Li, J. B., He, M. S., Zhang, Y., Tian, Q. H.,
685 and Peng, J. F.: Drought variations in the eastern part of northwest China over the past two
686 centuries: evidence from tree rings, *Clim. Res.*, 38, 129–135,
687 <https://doi.org/10.3354/cr00781>, 2009.
- 688 Feng, W., Wang, K. L., and Jiang, H.: Influences of westerly wind inter-annual change on water
689 vapor transport over northwest china summer, *Plateau Meteorology*, 23, 270–275 (In
690 Chinese with English abstract), 2004.
- 691 Gao, S. Y., Lu, R. J., Qiang, M. R., Ha, S., Zhang, D. S., Chen, Y., and Xia, H.: Precipitation
692 variation recorded by tree-rings in the northern Tengger Desert of the last 140 years, *Chin.*
693 *Sci. Bull.*, 51, 326–331, <https://doi.org/10.1360/CSB2006-51-3-326>, 2006.
- 694 Gou, X. H., Gao, L. L., Deng, Y., Chen, F. H., Yang, M. X., and Still, C.: An 850 - year tree -
695 ring - based reconstruction of drought history in the western Qilian Mountains of
696 northwestern China, *Int. J. Climatol.*, 35, 3308–3319, <https://doi.org/10.1002/joc.4208>,
697 2015a.
- 698 Gou, X. H., Deng, Y., Gao, L. L., Chen, F. H., Cook, E., Yang, M. M., and Zhang, F.: Millennium
699 tree-ring reconstruction of drought variability in the eastern Qilian Mountains, northwest
700 China, *Climate Dynamics*, 45, 1761–1770, <https://doi.org/10.1007/s00382-014-2431-y>,
701 2015b.
- 702 Huang, L. X., Chen, J., Yang, K., Yang, Y. J., Huang, W., Zhang, X., and Chen, F. H.: The
703 northern boundary of the Asian summer monsoon and division of westerlies and monsoon
704 regimes over the Tibetan Plateau in present-day, *Science China Earth Sciences*, 66, 882–
705 893, <https://doi.org/10.1007/s11430-022-1086-1>, 2023.
- 706 Jiang, D. B. and Wang, H. J.: Natural interdecadal weakening of East Asian summer monsoon
707 in the late 20th century, *Chin. Sci. Bull.*, 50, 1923–1929, <https://doi.org/10.1360/982005->

- 708 36, 2005.
- 709 Jiang, P., Liu, H. Y., Wu, X. C., and Wang, H. Y.: Tree-ring-based SPEI reconstruction in central
710 Tianshan Mountains of China since A.D. 1820 and links to westerly circulation, *Int. J.*
711 *Climatol.*, 37, 2863–2872, <https://doi.org/10.1002/joc.4884>, 2017.
- 712 Jiang, W. J., Wang, G. C., Sheng, Y. Z., Shi, Z. M., and Zhang, H.: Isotopes in groundwater (^2H ,
713 ^{18}O , ^{14}C) revealed the climate and groundwater recharge in the Northern China, *Sci. Total*
714 *Environ.*, 666, 298–307, <https://doi.org/10.1016/j.scitotenv.2019.02.245>, 2019.
- 715 Kang, S. Y. and Yang, B.: Precipitation variability at the northern fringe of the Asian summer
716 monsoon in Northern China and its possible mechanism over the past 530 years,
717 *Quaternary Sciences*, 35, 1185–1193, <https://doi.org/10.11928/j.issn.1001-7410.2015.05.14>, 2015.
- 719 Kang, S. Y., Yang, B., and Qin, C.: Recent tree-growth reduction in north central China as a
720 combined result of a weakened monsoon and atmospheric oscillations, *Clim. Change*, 115,
721 519–536, <https://doi.org/10.1007/s10584-012-0440-6>, 2012.
- 722 Li, D. L., Shao, P. C., and Wang, H.: The position variations of the north boundary of East Asia
723 subtropical summer monsoon in 1951–2009, *Journal of Desert Research*, 33, 1511–1519
724 (In Chinese with English abstract), <https://doi.org/10.7522/j.issn.1000-694X.2013.00217>,
725 2013.
- 726 Li, J. L., Li, Z. R., Yang, J. C., Shi, Y. Z., and Fu, J.: Analyses on spatial distribution and
727 temporal variation of atmosphere water vapor over northwest China in summer of later 10
728 years, *Plateau Meteorology*, 31, 1574–1581 (In Chinese with English abstract), 2012.
- 729 Li, J. P. and Zeng, Q. C.: A new monsoon index, its interannual variability and related with
730 monsoon precipitation, *Climatic and Environmental Research*, 10, 351–365 (In Chinese
731 with English abstract), 2005.
- 732 Li, W. L., Wang, K. L., Fu, S. M., and Jiang, H.: The interrelationship between regional Westerly
733 index and the water vapor budget in Northwest China, *Journal of Glaciology and*
734 *Geocryology*, 30, 28–34 (In Chinese with English abstract), 2008.
- 735 Li, Y.: The pollen records from lake sediments and climate & lake model in the Marginal area
736 of Asian monsoon, Lanzhou University, Lanzhou, China, 2009.
- 737 Li, Z. X., Feng, Q., Song, Y., Wang, Q. J., Yang, J., Li, Y. G., Li, J. G., and Guo, X. Y.: Stable
738 isotope composition of precipitation in the south and north slopes of Wushaoling Mountain,
739 northwestern China, *Atmospheric Research*, 182, 87–101,
740 <https://doi.org/10.1016/j.atmosres.2016.07.023>, 2016.
- 741 Liang, E. Y., Liu, X. H., Yuan, Y. J., Qin, N. S., Fang, X. Q., Huang, L., Zhu, H. F., Wang, L.,
742 and Shao, X. M.: The 1920s drought recorded by tree rings and historical documents in
743 the semi-arid and arid areas of Northern China, *Clim. Change*, 79, 403–432,
744 <https://doi.org/10.1007/s10584-006-9082-x>, 2006.
- 745 Liu, J. B., Chen, J., Chen, S. Q., Yan, X. W., Dong, H. R., and Chen, F. H.: Dust storms in

- 746 northern China and their significance for the concept of the Anthropocene, *Science China*
 747 *Earth Sciences*, 65, 921–933, <https://doi.org/10.1007/s11430-021-9889-8>, 2022.
- 748 Liu, Y., Cai, Q. F., Ma, L. M., and An, Z. S.: Tree ring precipitation records from Baotou and
 749 the East Asia summer monsoon variations for the last 254 years, *Earth Sci. Front.*, 8, 91–
 750 97 (In Chinese with English abstract), [https://doi.org/10.3321/j.issn:1005-](https://doi.org/10.3321/j.issn:1005-2321.2001.01.012)
 751 2321.2001.01.012, 2001.
- 752 Liu, Y., Sun, C. F., Li, Q., and Cai, Q. F.: A *Picea crassifolia* tree-ring width-based temperature
 753 reconstruction for the Mt. Dongda region, Northwest China, and its relationship to large-
 754 scale climate forcing, *PLoS One*, 11, e0160963,
 755 <https://doi.org/10.1371/journal.pone.0160963>, 2016.
- 756 Liu, Y., Lei, Y., Sun, B., Song, H. M., and Li, Q.: Annual precipitation variability inferred from
 757 tree-ring width chronologies in the Changling–Shoulu region, China, during AD 1853–
 758 2007, *Dendrochronologia*, 31, 290–296, <https://doi.org/10.1016/j.dendro.2013.02.001>,
 759 2013.
- 760 Liu, Y., Won-Kyu, P., Cai, Q. F., Jung-Wook, S., and Hyun-Sook, J.: Monsoonal precipitation
 761 variation in the East Asia since A.D. 1840—tree-ring evidences from China and Korea,
 762 *Science in China Series D: Earth Sciences*, 46, 1031–1039,
 763 <https://doi.org/10.1007/BF02959398>, 2003.
- 764 Liu, Y., Ma, L. M., Cai, Q. F., An, Z. S., Liu, W. G., and Gao, L. Y.: Reconstruction of summer
 765 temperature (June–August) at Mt. Helan, China, from tree-ring stable carbon isotope
 766 values since AD 1890, *Science in China Series D: Earth Sciences*, 45, 1127–1136,
 767 <https://doi.org/10.1360/02yd9109>, 2002.
- 768 Liu, Y., Cai, Q. F., Liu, W. G., Yang, Y. K., Sun, J. Y., Song, H. M., and Li, X. X.: Monsoon
 769 precipitation variation recorded by tree-ring $\delta^{18}\text{O}$ in arid Northwest China since AD 1878,
 770 *Chemical Geology*, 252, 56–61, <https://doi.org/10.1016/j.chemgeo.2008.01.024>, 2008.
- 771 Liu, Y., Cai, Q. F., Shi, J. F., Hughes, M. K., Kutzbach, J. E., Liu, Z. Y., Ni, F. B., and An, Z. S.:
 772 Seasonal precipitation in the south-central Helan Mountain region, China, reconstructed
 773 from tree-ring width for the past 224 years, *Canadian Journal of Forest Research*, 35,
 774 2403–2412, <https://doi.org/10.1139/x05-168>, 2005.
- 775 Liu, Y., Shi, J. F., Shishov, V., Vaganov, E., Yang, Y. K., Cai, Q. F., Sun, J. Y., Wang, L., and
 776 Djanseitov, I.: Reconstruction of May–July precipitation in the north Helan Mountain,
 777 Inner Mongolia since A.D. 1726 from tree-ring late-wood widths, *Chin. Sci. Bull.*, 49,
 778 405–409, <https://doi.org/10.1007/BF02900325>, 2004.
- 779 Ma, L. M., Liu, Y., Cai, Q. F., and An, Z. S.: The precipitation records from tree-ring late wood
 780 width in the helan mountain, *Marine geology & Quaternary geology*, 23, 109–114 (In
 781 Chinese with English abstract), <https://doi.org/10.16562/j.cnki.0256-1492.2003.04.016>,
 782 2003.
- 783 Ma, M. J., Pu, Z. X., Wang, S. G., and Zhang, Q. A.: Characteristics and numerical simulations
 784 of extremely large atmospheric boundary-layer heights over an arid region in north-west

- 785 china, *Boundary-Layer Meteorology*, 140, 163–176, [https://doi.org/10.1007/s10546-011-](https://doi.org/10.1007/s10546-011-9608-2)
786 9608-2, 2011.
- 787 Ma, Z. G. and Fu, C. B.: The basic facts of aridity in northern China from 1951 to 2004, *Chin.*
788 *Sci. Bull.*, 51, 2429–2439 (In Chinese), <https://doi.org/10.1360/csb2006-51-20-2429>,
789 2006.
- 790 Ou, T. H. and Qian, W. H.: Vegetation variations along the monsoon boundary zone in East
791 Asia, *Chinese Journal of Geophysics*, 49, 698–705 (In Chinese with English abstract),
792 2006.
- 793 Qin, L., Liu, G. X., Li, X. Z., Chongyi, E., Li, J., Wu, C. R., Guan, X., and Wang, Y.: A 1000-
794 year hydroclimate record from the Asian summer monsoon-Westerlies transition zone in
795 the northeastern Qinghai-Tibetan Plateau, *Clim. Change*, 176, 1–20, [https://doi.org](https://doi.org/10.1007/s10584-023-03497-1)
796 [/10.1007/s10584-023-03497-1](https://doi.org/10.1007/s10584-023-03497-1), 2023.
- 797 Qu, W. J., Zhang, X. H., Wang, D., Shen, Z. X., Mei, F. M., Cheng, Y., and Yan, L. W.: The
798 important significance of westerly wind study, *Marine Geology and Quaternary Geology*,
799 24, 125–132 (In Chinese with English abstract), [https://doi.org/10.16562/j.cnki.0256-](https://doi.org/10.16562/j.cnki.0256-1492.2004.01.018)
800 1492.2004.01.018, 2004.
- 801 Shao, X. M., Xu, Y., Yin, Z. Y., Liang, E. Y., Zhu, H. F., and Wang, S.: Climatic implications of
802 a 3585-year tree-ring width chronology from the northeastern Qinghai-Tibetan Plateau,
803 *Quaternary Science Reviews*, 29, 2111–2122,
804 <https://doi.org/10.1016/j.quascirev.2010.05.005>, 2010.
- 805 Sun, D. H., An, Z. S., Su, R. H., Deer, H. Y., and Sun, Y. B.: The dust deposition records of the
806 evaluation of Asia monsoon and Westerly circulation in north China in the last 2.6Ma,
807 *Science in China (Series D)*, 33, 497–504 (In Chinese), 2003.
- 808 Sun, L. Q., Li, T. J., Li, Q. L., and Wu, Y. P.: Responses of autumn flood peak in the Yellow
809 River source regions to westerly circulation index, *Journal of Glaciology and Geocryology*,
810 41, 1475–1482 (In Chinese with English abstract), [https://doi.org/10.7522/j.issn.1000-](https://doi.org/10.7522/j.issn.1000-0240.2019.0028)
811 0240.2019.0028, 2019.
- 812 Tang, X., Qian, W. H., and Liang, P.: Climatic features of boundary belt for East Asian Summer
813 Monsoon, *Plateau Meteorology*, 25, 375–381 (In Chinese with English abstract), 2006.
- 814 Vicente-Serrano, S.M., Beguería, S. and López-Moreno, J.I.: A multiscalar drought index
815 sensitive to global warming: the standardized precipitation evapotranspiration index. *J.*
816 *Clim.*, 23(7): 1696–1718, <https://doi.org/10.1175/2009jcli2909.1>, 2010.
- 817 Wang, B. J., Huang, Y. X., He, J. H., and Wang, L. J.: Relation between vapour transportation
818 in the period of East Asian Summer Monsoon and drought in Northwest China. *Plateau*
819 *Meteorology*, 23, 912–917 (In Chinese with English abstract), 2004.
- 820 Wang, J. L., Yang, B., Ljungqvist, F. C., Luterbacher, J., Osborn, Timothy j., Briffa, K. R., and
821 Zorita, E.: Internal and external forcing of multidecadal Atlantic climate variability over
822 the past 1,200 years, *Nature Geoscience*, 10, 512–517, <https://doi.org/10.1038/ngeo2962>,
823 2017.

- 824 Wang, K. L., Jiang, H., and Zhao, H. Y.: Atmospheric water vapor transport from westerly and
825 monsoon over the Northwest China, *Advances in Water Science*, 16, 432–438 (In Chinese
826 with English abstract), <https://doi.org/10.14042/j.cnki.32.1309.2005.03.021>, 2005.
- 827 Wigley, T.M.L., Briffa, K.R., Jones, P.D. On the average value of correlated time series, with
828 applications in dendroclimatology and hydrometeorology. *Journal of Climate and Applied
829 Meteorology* 23(2), 201–213, 1984.
- 830 Xiao, S. C., Chen, X. H., and Ding, A. J.: Study process of climate changes, environment
831 evolution and its driving mechanism in the last two centuries in the Alxa Desert, *Journal
832 of Desert Research*, 37, 1102–1201 (In Chinese with English abstract),
833 10.7522/j.issn.1000-694x.2017.00002, 2017.
- 834 Xiao, S. C., Yan, C. Z., Tian, Y. Z., Si, J. H., Ding, A. J., Chen, X. H., Han, C., and Teng, Z. Y.:
835 Regionalization for desertification control and countermeasures in the Alxa Plateau, China,
836 *Journal of Desert Research*, 39, 182–192 (In Chinese with English abstract),
837 <https://doi.org/10.7522/j.issn.1000-694X.2019.00068>, 2019.
- 838 Xu, J. J., Wang, K. L., Jiang, H., Li, Z. G., Sun, J., Luo, X. P., and Zhu, Q. L.: A numerical
839 simulation of the effects of Westerly and Monsoon on precipitation in the Heihe River
840 Basin, *Journal of Glaciology and Geocryology*, 32, 489–496 (In Chinese with English
841 abstract), 2010.
- 842 Yan, H. S., Hu, J., Fan, K., and Zhang, Y. J.: The analysis of relationship between the variations
843 of Westerly Index in summer and precipitation during the flood period over China in the
844 last 50 years. , *Chinese Journal of Atmospheric Science*, 31, 717–726 (In Chinese with
845 English abstract), 2007.
- 846 Yang, B., Qin, C., Wang, J. L., He, M. H., Melvin, T. M., Osborn, T. J., and Briffa, K. R.: A
847 3,500-year tree-ring record of annual precipitation on the northeastern Tibetan Plateau,
848 *Proc. Natl. Acad. Sci. USA*, 111, 2903–2908, <https://doi.org/10.1073/pnas.1319238111>,
849 2014.
- 850 Yang, J. H., Zhang, Q., Liu, X. Y., Yue, P., Shang, J. L., Ling, H., and Li, W. J.: Spatial-temporal
851 characteristics and causes of summer precipitation anomalies in the transitional zone of
852 typical summer monsoon, China, *Chinese Journal of Geophysics*, 62, 4120–4128 (In
853 Chinese with English abstract), <https://doi.org/10.6038/cjg2019M0639>, 2019.
- 854 Yuan, L.: *Hazards history in northwestern China*, Gansu people's press, Lanzhou, China 1994.
- 855 Zhang, F., Chen, Q. M., Su, J. J., Deng, Y., Gao, L. L., and Gou, X. H.: Tree-ring recorded of
856 the drought variability in the northwest monsoon marginal, China, *Journal of Glaciology
857 and Geocryology*, 39, 245–251 (In Chinese with English abstract),
858 <https://doi.org/10.7522/j.issn.1000-0240.2017.0028>, 2017.
- 859 Zhang, Q., Yang, J. H., Wang, P. L., Yu, H. P., Yue, P., Liu, X. Y., Lin, J. J., Duan, X. Y., Zhu,
860 B., and Yan, X. Y.: Progress and prospect on climate warming and humidification in
861 Northwest China, *Chin. Sci. Bull.*, 68, 1814–1828, <https://doi.org/10.1360/TB-2022-0643>,
862 2023.

- 863 Zhang, Q. B., Cheng, G. D., Yao, T. D., Kang, X. C., and Huang, J. G.: A 2,326 year tree-ring
864 record of climate variability on the northeastern Qinghai-Tibetan Plateau, *Geophys. Res.*
865 *Let.*, 30, 1739, <https://doi.org/10.1029/2003GL017425>, 2003.
- 866 Zhang, Q. L., Liu, W. G., Liu, Y., Ning, Y. F., and Wen, Q. B.: Relationship between the stable
867 carbon and oxygen isotopic compositions of tree ring in the Mt. Helan region,
868 Northwestern China, *Geochimica*, 34, 51–56, [https://doi.org/10.19700/j.0379-](https://doi.org/10.19700/j.0379-1726.2005.01.006)
869 1726.2005.01.006, 2005a.
- 870 Zhang, S., Xu, H., Lan, J. H., Goldsmith, Y., Torfstein, A., Zhang, G. L., Zhang, J., Song, Y. P.,
871 Zhou, K. E., Tan, L. C., Xu, S., Xu, X. M., and Enzel, Y.: Dust storms in northern China
872 during the last 500 years, *Science China Earth Sciences*, 64, 813–824,
873 <https://doi.org/10.1007/s11430-020-9730-2>, 2021.
- 874 Zhang, Y., Shao, X. M., Yin, Z. Y., Liang, E. Y., Tian, Q. H., and Xu, Y.: Characteristics of
875 extreme droughts inferred from tree-ring data in the Qilian Mountains, 1700-2005, *Clim.*
876 *Res.*, 50, 141–159, <https://doi.org/10.3354/cr01051>, 2011.
- 877 Zhang, Y. X., Yu, L., and Yin, H.: Annual precipitation reconstruction over last 191 years at the
878 south edge of Badain Jaran Desert based on tree ring width data, *Desert and Oasis*
879 *Meteorology*, 9, 12–16 (In Chinese with English abstract),
880 <https://doi.org/10.3969/j.issn.1002-0799.2015.01.003>, 2015.
- 881 Zhang, Y. X., Gou, X. H., Hu, W. D., Peng, J. F., and Liu, P. X.: The drought events recorded
882 in tree ring width in Helan Mt. over past 100 years, *Acta Ecologica Sinica*, 25, 2121–2126
883 (In Chinese with English abstract), 2005b.
- 884